Ferromagnetic Interaction between Aminium Radical Centers through *m*-Phenylene and *m*-1,3,5-Triazinediyl

Akihiro Ito,[†] Hiroki Miyajima,[†] Kazunari Yoshizawa,[†] Kazuyoshi Tanaka,[†] and Tokio Yamabe*,[†,‡]

Department of Molecular Engineering, School of Engineering, Kyoto University, Sakyo-ku, Kyoto 606-01, Japan, and Institute for Fundamental Chemistry, 34-4 Takano-Nishihiraki-cho, Sakyo-ku, Kyoto 606, Japan

Received June 3, 1996[⊗]

Ab initio MO study (at the ROHF, GVB, and CASSCF levels) of *m*-phenylenediamine (**1**) and 2,4-diamino-1,3,5-triazine (**2**) dication diradicals, which are model molecules of two possible high-spin polymers, poly(*m*-aniline) and poly(imino-1,3,5-triazinediyl) cation radicals, is presented. On the basis of qualitative MO considerations, it was seen that the electronic structures of $\mathbf{1}^{2+}$ and $\mathbf{2}^{2+}$ differed considerably. The singlet−triplet splittings (ΔE_{S-T}) of $\mathbf{1}^{2+}$ and $\mathbf{2}^{2+}$ were calculated to be 0.7 and 12.5 kcal/mol, respectively, at the CASPT2 level. *m*-1,3,5-Triazinediyl is shown to be a strong ferromagnetic coupler for aza-substituted systems.

Introduction

Since the experimental verification by Itoh and Wasserman *et al.*[1] and Mataga's proposition,[2] much attention has been given to the chemistry of organic high-spin molecules and, in particular, the possibility of organic ferromagnets consisting of *m*-phenylene and several radical centers.[3] In the simple Hückel MO theory, *m*-quinodimethane (*m*-QDM) has two degenerate nonbonding MOs (NBMO); according to Hund's rule, the two frontier electrons separately occupy these two NBMOs to lead to a ground-state triplet. Borden and Davidson[4] confirmed topology rules predicting the spin preference of alternant hydrocarbon π-systems. Supported by these rules, many di- and polyradicals have revealed that *m*-phenylene is a robust ferromagnetic coupler for the realization of high-spin organic molecules.[3]

As is well known,[5] kinetically and thermally *stable* polyradicals contain heteroatoms that can become spin-containing sites. However, the possibility exists that heteroatom perturbation lifts the degeneracy of NBMOs, and hence, the above-mentioned rules are not pertinent to heteroatom-containing systems. On the basis of ESR studies and *ab initio* MO calculations,[6,7] it was shown that heteroatom substitution causes the spin preference for a low-spin state.[8] In particular, Dougherty *et al.*[7] clarified recently that some aza-substituted *m*-phenylenes and, particularly, their protonated forms lead to antiferromagnetic interaction between such radical centers when the N-atoms are effectively substituted in order to perturb one NBMO relative to the other. When N-atom-containing spin sites are attached to a robust ferromagnetic coupling unit such as 1,3- or 1,3,5-connected benzene, on the other hand, Dougherty *et al.*[7] and other research groups[9−11] reported that high-spin states are maintained due to quasidegenerate NBMOs. In addition, Müllen *et al.*[12] pointed out recently, using a semiempirical MO method, that *m*-1,3,5-triazinediyl is another strong ferromagnetic coupler. In this context, we report here on the electronic structures of *m*-phenylenediamine (**1**) and 2,4-diamino-1,3,5-triazine (**2**) dication diradicals (Chart 1), which are the model molecules of two possible high-spin polymers, poly(*m*-aniline)[9,13] and poly(imino-1,3,5-triazinediyl) cation radicals, using the *ab initio* MO method.

Chart 1

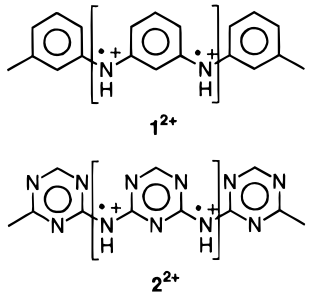

Prior to the description of detailed calculation results, let us look at the NBMOs of **1** and **2**, although their

[†] Kyoto University.
[‡] Institute for Fundamental Chemistry.
[⊗] Abstract published in *Advance ACS Abstracts,* December 15, 1996.

(1) Itoh, K. *Chem. Phys. Lett.* **1967**, *1*, 235−238. Wasserman, E.; Murray, R. W.; Yager,W. A.; Trozzolo, A. M.; Smolinsky, G. *J. Am. Chem. Soc.* **1967**, *89*, 5076−5078.
(2) Mataga, N. *Theor. Chim. Acta* **1968**, *10*, 372−376.
(3) Rajca, A. *Chem. Rev.* **1994,** *94*, 871−893 and references therein.
(4) Borden, W. T.; Davidson, E. R. *J. Am. Chem. Soc.* **1977**, *99*, 4587−4594. Borden, W. T. In *Diradicals*: Borden, W. T., Ed. Wiley: New York, 1982; pp 1−72.
(5) Forrester, A. R.; Hay, J. M.; Thomson, R. H. *Organic Chemistry of Stable Free Radicals*; Academic Press: New York, 1968.
(6) Gleiter, R.; Hoffmann, R. *Angew. Chem., Int. Ed. Engl.* **1969**, *8*, 214−215. Du, P.; Hrovat, D. A.; Borden, W. T. *J. Am. Chem. Soc.* **1989**, *111*, 3773−3778. Greenberg, M. M.; Blackstock, S. C.; Berson, J. A.; Merrill, R. A.; Duchamp, J. C.; Zilm, K. W. *J. Am. Chem. Soc.* **1991**, *113*, 2318−2319. Hirano, T.; Kumagai, T.; Miyashi, T. *J. Org. Chem.* **1992**, *57*, 876−882.
(7) West, A. P., Jr.; Silverman, S. K.; Dougherty, D. A. *J. Am. Chem. Soc.* **1996**, *118*, 1452−1463.
(8) This situation is not a *violation* of the high-spin topology rules; appropriate rules may be reconstructed for heteroatom-containing systems.
(9) Tyutyulkov, N.; Polansky, O. E. *Chem. Phys. Lett.* **1989**, *139*, 281−283. Baumgarten, M.; Müllen, K.; Tyutyulkov, N.; Madjarova, G. *Chem. Phys.* **1993**, *169*, 81−84. Madjarova, G.; Baumgarten, M.; Müllen, K.; Tyutyulkov, N. *Macromol. Theory Simul.* **1994**, *3*, 803−815.
(10) Berson, J. A. In *The Chemistry of Quinoid Compounds*; Patai, S., Rappaport, Z., Eds.; Wiley: New York, 1988; Vol. 2, Chapter 10. Fort, R. C., Jr.; Getty, S. J.; Hrovat, D. A.; Lahti, P. M.; Borden, W. T. *J. Am. Chem. Soc.* **1992**, *114*, 7549−7552.
(11) Yoshizawa, K.; Hatanaka, M.; Ito, A.; Tanaka, K.; Yamabe, T. *Chem. Phys. Lett.* **1993**, *202*, 483−488. Yoshizawa, K.; Hatanaka, M.; Matsuzaki, Y.; Tanaka, K.; Yamabe, T. *J. Chem. Phys.* **1994**, *100*, 4453−4458.
(12) Müllen, K.; Baumgarten, M.; Tyutyulkov, N.; Dietz, F. *Mol. Eng.* **1995**, *4*, 353−367.
(13) Yoshizawa, K.; Hoffmann, R. *Chem. Eur. J.* **1995**, *1*, 403−413.

S0022-3263(96)01031-6 CCC: $14.00

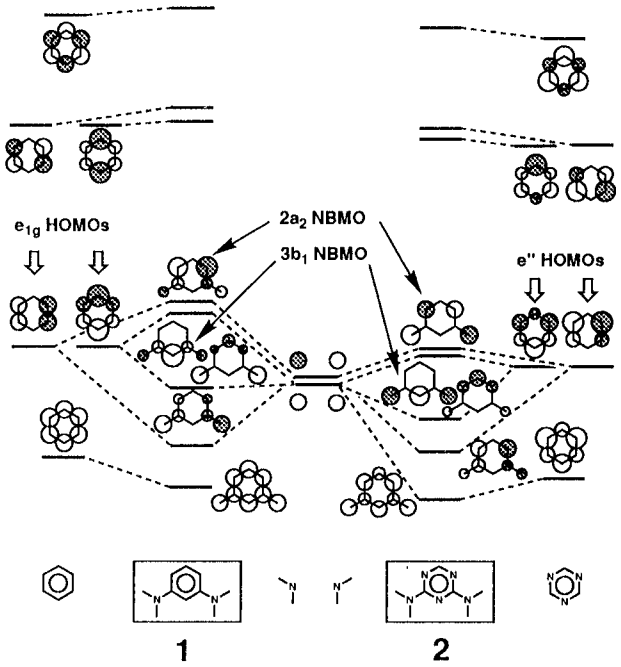

Figure 1. Fragment MO correlation diagram for **1** (left) and **2** (right).

Chart 2

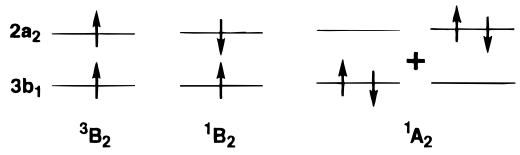

nonbonding character is not exactly maintained, due to aza-substitution. As illustrated by the qualitative π-MO correlation diagram shown in Figure 1, N atom perturbation clearly changes the whole situation as compared with *m*-QDM. The NBMOs of **1** (or **2**) are composed of an out-of-phase combination of the benzene e_{1g} (or the 1,3,5-triazine e″) HOMOs and the π-orbitals of two amino groups. However, the electron density of the NBMOs of **1** resides in the benzene ring because the energy level of the benzene e_{1g} HOMOs lies above the π-MOs of the two amino groups. On the other hand, the energy level of the 1,3,5-triazine e″ HOMOs is lowered to that of the amino groups, so that **2** recovers the electron density on the peripheral N atoms like *m*-QDM. This means that $\mathbf{2}^{2+}$ has a more localized diradical character than $\mathbf{1}^{2+}$. Figure 1 shows another facet of spin preference, due to heteroatom substitution, in contrast to the results of Dougherty *et al.*[7]

Computational Details

Full geometry optimizations in C_{2v} symmetry were carried out for the three lowest lying states ($^3B_2$, $^1B_2$, $^1A_1$) of $\mathbf{1}^{2+}$ and $\mathbf{2}^{2+}$ using the 6-31G* basis set.[14] This basis represents a compromise between completeness and economy; it includes polarization functions on non-hydrogen atoms useful for modeling radicals and then delivers reasonable geometries and physical properties.[14,15] At the zeroth approximation, these states correspond to different occupations of the two frontier electrons into the two NBMOs, $3b_1$ and $2a_2$ (Figure 1), as shown in Chart 2. The $^3B_2$ state is reasonably described by a single configuration of $|...3b_1{}^1 2a_2{}^1(\alpha\alpha)\rangle$. In the $^1B_2$ state, the frontier electrons are occupied as in the $^3B_2$ state, but their spins form a configuration of $|...3b_1{}^1 2a_2{}^1(\alpha\beta-\beta\alpha)/\sqrt{2}\rangle$. On the other hand, the $^1A_1$ state is represented by a two-configuration (TC) wavefunction such as $c_1{}^2|...3b_1{}^2\rangle - c_2{}^2|...2a_2{}^2\rangle$, where the coefficients c_1 and c_2 represent the indices of the localized diradical character as described below. We thus treated the $^3B_2$ and $^1B_2$ states with the restricted open-shell HF (ROHF) method[16] and the $^1A_1$ with the generalized valence bond (GVB) method.[17] All the calculated structures except for that of the $^1B_2$ state[18] were characterized as local minimum structures (no imaginary frequency) by evaluation of the second derivatives of the energy at the ROHF(or GVB)/6-31G* level.

It is well-known that electron correlation can be partially provided for the triplet states by carrying out the UHF calculations in which electrons of different spin are allowed to occupy different MOs. However, it is also pointed out that the UHF calculations often lead to a mixture of spin states so that the UHF wavefunctions are contaminated by states of higher spin multiplicities and are not eigenfunctions of the S^2 operator. Therefore, the UHF calculations do not provide a generally useful method for obtaining correlated wavefunctions from which the relative energies of the low-lying states in diradicals can be investigated.[19] On the other hand, the ROHF method gives wavefunctions with a pure spin state and treats correctly the different Coulomb repulsion energies of the triplet ($^3B_2$) and corresponding singlet ($^1B_2$) states[4,20] although no electron correlation is included in the method.

In order to represent the $^1A_1$ state, the above-mentioned TCSCF wavefunction is required. The TC wavefunction above can be factored into

$$|...(c_1 3b_1 + c_2 2a_2)(c_1 3b_1 - c_2 2a_2)(\alpha\beta - \beta\alpha)/\sqrt{2}\rangle$$

where the singly occupied, nonorthogonal-sum and -difference orbitals are referred to as GVB orbitals. Once the nonorthogonal GVB orbitals are obtained variationally, the final coefficients, c_1 and c_2, are provided along with the overlapping singlet coupled orbitals corresponding to each pair of the GVB orbitals. When the GVB orbitals are partially confined to different regions of space, the GVB wavefunction contains fewer ionic terms than the RHF wavefunction that is obtained by setting $c_2 = 0$. To put it another way, a picture of the singlet diradical can be realized. This is a major advantage of a GVB wavefunction over a one-configuration MO description. However, the GVB wavefunction for the $^1A_1$ state provides no correlation between the two frontier electrons and those in the bonding π-MOs.[4]

Although RHF/GVB calculations treat correctly the Coulomb interactions between the two frontier electrons in diradicals, an accurate calculation of the relative state energies requires the inclusion of electron correlation. Correlated wavefunctions for pure spin states are obtained by linear combinations of electron configurations. Such multiconfigurational (MC) wavefunctions can be obtained directly by MCSCF calculations.[21] The MCSCF wavefunction is represented by "truncated" configuration interaction (CI) expansion as

$$|\Psi_{\mathrm{MCSCF}}\rangle = \sum_{\mathrm{I}} c_{\mathrm{I}} |\Psi_{\mathrm{I}}\rangle$$

where c_{I} is the CI expansion coefficient and Ψ_{I} is the config-

(14) Hehre, W. J.; Radom, L.; Schleyer, P. v. R.; Pople, J. A. *Ab Initio Molecular Orbital Theory*; Wiley: New York, 1986.
(15) Davidson, E. R.; Feller, D. *Chem. Rev.* **1986**, *86*, 681−696.
(16) McWeeny, R.; Dierkson, G. *J. Chem. Phys.* **1968**, *49*, 4852−4856.
(17) Bobrowicz, F. W.; Goddard, W. A., III. In *Methods of Electronic Structure Theory*; Schaefer, H. F., III, Ed.; Plenum: New York, 1977; pp 79−126.
(18) As for the $^1B_2$ state, it was difficult to obtain the optimized geometry, as described by ref 7, and hence, trial-and-error was needed for both $\mathbf{1}^{2+}$ and $\mathbf{2}^{2+}$.
(19) The $\langle S^2\rangle$ values (2.0 for pure triplets) for the UHF/6-31G*-optimized $^3B_2$ states for $\mathbf{1}^{2+}$ and $\mathbf{2}^{2+}$ were 2.473 and 2.695, respectively.
(20) There is a suggestion that the UHF method is preferred to the ROHF method for optimizing the geometries of triplet states; see, for instance: Borden, W. T.; Davidson, E. R.; Feller, D. *Tetrahedron* **1982**, *38*, 737−739.
(21) Wahl, A. C.; Das, G. In *Methods of Electronic Structure Theory*; Schaefer, H. F., III, Ed.; Plenum: New York, 1977; p 51.

Table 1. Optimized Bond Lengths (Å) and Angles (Deg) of 1^{2+} and 2^{2+}

	$^3B_2$		$^1B_2$		$^1A_1$	
parameter	ROHF	CASSCF	ROFH	CASSCF	GVB	CASSCF
1^{2+}						
C1−C2	1.382	1.394	1.382	1.396	1.376	1.386
C2−C3	1.440	1.441	1.450	1.456	1.480	1.467
C3−C4	1.455	1.447	1.472	1.468	1.383	1.393
N1−C3	1.292	1.306	1.282	1.290	1.316	1.323
C2−C1−C6	122.7	122.2	123.3	123.0	117.5	118.0
C1−C2−C3	120.3	119.9	120.3	120.1	121.8	121.4
C2−C3−C4	118.7	119.5	118.7	118.8	120.1	120.2
C3−C4−C5	119.3	118.9	118.7	119.3	118.8	118.8
N1−C3−C4	119.7	119.5	119.6	119.7	124.1	123.9
2^{2+}						
C1−N1	1.328	1.335	1.319	1.334	1.328	1.336
N1−C2	1.298	1.351	1.376	1.392	1.297	1.314
C2−N2	1.311	1.352	1.414	1.397	1.309	1.323
C2−N4	1.418	1.330	1.264	1.281	1.424	1.410
N1−C1−N3	122.4	123.0	124.4	124.5	122.3	122.2
C1−N1−C2	115.1	116.4	118.1	117.1	115.1	115.6
N1−C2−N2	128.2	125.8	123.4	124.2	128.3	127.6
C2−N2−N3	111.0	112.6	112.5	112.9	110.9	111.5
N2−C2−N4	116.3	117.0	117.3	117.3	116.6	117.0

uration state function, which must be appropriately selected according to the molecular system considered. Herein, both c_I and MO coefficients in Ψ_I are simultaneously optimized.[21] In the complete active space SCF (CASSCF) method,[22] all linear independent configurations generated from all possible occupations in an active orbital space were utilized by MCSCF calculations, and furthermore, technical difficulties were overcome compared with the conventional MCSCF method. The accuracy of this method is proved by the results of calculations in well-established systems.[23]

In order to correct the ROHF/GVB results, we thus included electron correlation using the CASSCF method with the 6-31G* basis set and took account of all configurations that arise when eight electrons are allowed to occupy eight π-orbitals corresponding to the eight Hückel π-MOs shown in Figure 1. Thus, the active space orbitals adopted here were $1b_1 1a_2 2b_1 3b_1 2a_2 4b_1 3a_2 5b_1$ (for the $^1A_1$ state of $\mathbf{1}^{2+}$, $4b_1$ and $3a_2$ orbitals are inverted), and led to 1764 configurations for the $^1A_1$ and $^1B_2$ states and to 2352 for the $^3B_2$ state. These CAS(8,8) (or π-CAS) calculations were carried out at the ROHF/GVB optimized geometries. Incidentally, the ROHF/GVB method is equivalent to the CAS(2,2) method. Moreover, these three states were reoptimized at the same CASSCF level. All calculations were performed with the Gaussian 94 package of *ab initio* MO programs.[24]

Results and Discussion

The optimized bond lengths and angles of $\mathbf{1}^{2+}$ and $\mathbf{2}^{2+}$ are listed in Table 1. The atoms of $\mathbf{1}^{2+}$ and $\mathbf{2}^{2+}$ are labeled in Chart 3. In contrast to *m*-QDM,[10,25] the triplet state of $\mathbf{1}^{2+}$ has a strong C−N π-bonding character (1.292 Å) owing to N atom substitution. The $^1B_2$ state takes an equilibrium geometry similar to that for the $^3B_2$ state. In the $^1B_2$ state, unlike the case in the $^3B_2$, the frontier electrons are not prevented, due to the Pauli exclusion

Chart 3

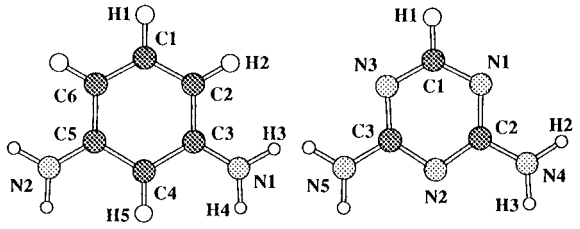

$\mathbf{1}^{2+}$ $\mathbf{2}^{2+}$

principle, from appearing in the same region of space. Hence, the frontier electrons of the $^1B_2$ state are more localized on different regions of space over the benzene ring than those of the $^3B_2$ state in order to minimize the Coulomb repulsion.[4,10] This is indicated by the shorter C−N bond length (1.282 Å). The ROHF/GVB and CASSCF methods give close geometrical parameters for the $^3B_2$ and $^1B_2$ states. In contrast, the $^1A_1$ geometry gives signs of "cyanine distortion",[26] which produces the six-membered ring dication with two cyanine-like subunits. In 1,2,4,5-tetrakis(dimethylamino)benzene dication, the cyanine distortion is realized at the expense of aromaticity.[27] However, at the ROHF/GVB level, the planar optimized structure is a local minimum, and moreover, we could not find a full cyanine-distorted structure. From the Mulliken atomic charge analysis, the major part of the charge in the $^1A_1$ state was found to be concentrated in one of the two cyanine-like subunits. More noteworthy is that the $^1A_1$ state has closed-shell character (c_1 and c_2 are 0.9624 and 0.2715, respectively). This electronic structure is certainly responsible for the wide energy gap between the two NBMOs. As shown in Table 2, the ROHF/GVB energy gap (5.17 eV) between the $3b_1$ and $2a_2$ MOs is considerably large compared with the other states. Major variations in the C2−C3 bond length and bond angles were not found in going from the ROHF/GVB level to the CASSCF level.

At the ROHF/GVB level, the $^3B_2$ state is predicted to be the ground state of $\mathbf{1}^{2+}$, which lies 3.9 kcal/mol below

(22) Roos, B. O. *Adv. Chem. Phys.* **1987**, *69*, 399−445.
(23) See, for recent examples: Hrovat, D. A.; Borden, W. T. *J. Am. Chem. Soc.* **1994**, *116*, 6327−6331. Liu, R.; Morokuma, K.; Mebel, A. M.; Lin, M. C. *J. Phys. Chem.* **1996**, *100*, 9314−9322.
(24) Frisch, M. J.; Trucks, G. W.; Schlegel, H. B.; Gill, P. M. W.; Johnson, B. G.; Robb, M. A.; Cheeseman, J. R.; Keith, T. A.; Peterson, G. A.; Montgomery, J. A.; Raghavachari, K.; Al-Laham, M. A.; Zakrzewski, V. G.; Ortiz, J. V.; Foresman, J. B.; Cioslowski, J.; Stefanov, B. B.; Nanayakkara, A.; Challacombe, M.; Peng, C. Y.; Ayala, P. Y.; Chen, W.; Wong, M. W.; Andres, J. L.; Replogle, E. S.; Gomperts, R.; Martin, R. L.; Fox, P. J.; Binkley, J. S.; Defrees, D. J.; Baker, J.; Stewart, J. P.; Head-Gordon, M.; Gonzalez, C.; Pople, J. A. *Gaussian 94*, Revision A.1; Gaussian, Inc., Pittsburg, PA, 1995.
(25) Kato, S.; Morokuma, K.; Feller, D.; Davidson, E. R.; Borden, W. T. *J. Am. Chem. Soc.* **1983**, *105*, 1791−1795.
(26) Bock, H.; Ruppert, K.; Näther, C.; Havlas, Z.; Herrmann, H.-F.; Arad, C.; Göbel, I.; John, A.; Meuret, J.; Nick, S.; Rauschenbach, A.; Seitz, W.; Vaupel, T.; Solouki, B. *Angew. Chem., Int. Ed. Engl.* **1992**, *31*, 550−581.
(27) Elbl, K.; Krieger, C.; Staab, H. A. *Angew. Chem., Int. Ed. Engl.* **1986**, *25*, 1023−1024.

Table 2. Energy Difference[a] (eV) between Two NBMO's of 1^{2+}, 2^{2+}, and *m*-QDM at the ROHF/GVB Level

	$^3B_2$	$^1B_2$	$^1A_1$
$\mathbf{1}^{2+}$	0.68	3.09	5.17
$\mathbf{2}^{2+}$	0.26	3.30	0.70
m-QDM	0.04	0.01	0.32

[a] $2a_2$ orbital energy − $3b_1$ orbital energy.

Table 3. Energies of the Triplet and Singlet States of 1^{2+} and 2^{2+}

	state	geometry	calculation	*E*/hartree	E_{rel}[a]/kcal/mol
$\mathbf{1}^{2+}$					
	$^3B_2$	ROHF	ROHF	−340.1096	0
		ROHF	CASSCF	−340.1991	0
		CASSCF	CASSCF	−340.2000	0
		CASSCF	CASPT2	−341.0968	0
	$^1B_2$	ROHF	ROHF	−340.0953	9.0
		ROHF	CASSCF	−340.1828	10.2
		CASSCF	CASSCF	−340.1835	10.4
		CASSCF	CASPT2	−341.0790	11.2
	$^1A_1$	GVB	GVB	−340.1034	3.9
		GVB	CASSCF	−340.1717	17.2
		CASSCF	CASSCF	−340.1723	17.4
		CASSCF	CASPT2	−341.0957	0.7
$\mathbf{2}^{2+}$					
	$^3B_2$	ROHF	ROHF	−388.0152	0
		ROHF	CASSCF	−388.1102	0
		CASSCF	CASSCF	−388.1206	0
		CASSCF	CASPT2	−389.0589	0
	$^1B_2$	ROHF	ROHF	−387.9828	20.3
		ROHF	CASSCF	−388.0893	13.1
		CASSCF	CASSCF	−388.0911	18.5
		CASSCF	CASPT2	−389.0340	15.6
	$^1A_1$	GVB	GVB	−388.0135	1.1
		GVB	CASSCF	−388.0545	34.9
		CASSCF	CASSCF	−340.1723	12.8
		CASSCF	CASPT2	−389.0389	12.5

[a] Energy relative to the triplet state, where the positive value represents triplet < singlet.

the $^1A_1$ state. The $^1B_2$ state lies 5.1 kcal/mol above the $^1A_1$ state. At the CASSCF level, the lowest singlet state of $\mathbf{1}^{2+}$ changes from $^1A_1$ to $^1B_2$ as shown in Table 3. This is because the benzene ring in the $^1A_1$ geometry is considerably distorted from a regular hexagon, due to cyanine-like distortion; hence, it is less stabilized by the CASSCF treatment. The energy difference between the $^3B_2$ and $^1B_2$ states also remains unchanged in the CASSCF method since the two states have similar geometries. Indeed, the fractional occupation numbers of the $^3B_2$ state (1.95, 1.94, 1.89, 1.00, 1.00, 0.10, 0.07, 0.04) and the $^1B_2$ state (1.95, 1.94, 1.90, 1.01, 1.01, 0.10, 0.05, 0.04) that are obtained from the CASSCF//CASSCF calculations show a similar tendency. Consequently, at the CASSCF//CASSCF level, the triplet state is predicted to be lower in energy than $^1B_2$ in $\mathbf{1}^{2+}$, following the high-spin topology rules[4] of the quasidegenerate *nondisjoint* NBMOs.

Let us turn to $\mathbf{2}^{2+}$. From the Mulliken atomic charge analysis, the charge density on $\mathbf{2}^{2+}$ was found to be extensively polarized over the triazine ring in all the states compared to that on $\mathbf{1}^{2+}$.[28] At the ROHF/GVB level, despite the energy lowering of e" HOMO of 1,3,5-triazine, in the $^1B_2$ state of $\mathbf{2}^{2+}$, the frontier electrons are similarly localized as in the $^1B_2$ state of $\mathbf{1}^{2+}$. At the CASSCF level, there were no noticeable changes in

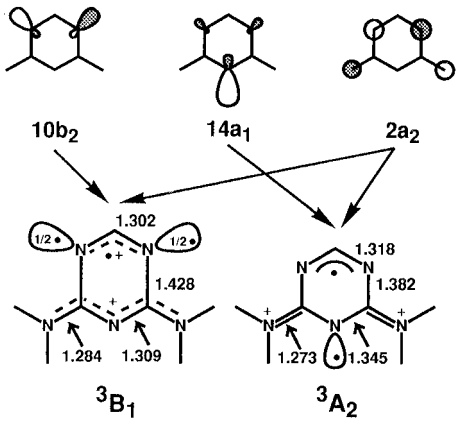

Figure 2. Bond lengths (Å) and schematic spin and charge distributions for the $^3B_1$ and $^3A_2$ states of $\mathbf{2}^{2+}$.

reoptimized geometrical parameters. On the other hand, the $^3B_2$ and $^1A_1$ states have a diradical character localized mainly on the peripheral N atoms; in the $^1A_1$ state, c_1 and c_2 are 0.7316 and 0.6816, respectively. In addition, the exocyclic C2−N4 distance is noticeably longer and close to that of a typical C−N single bond both in the $^3B_2$ state and in the $^1A_1$ state. Unexpectedly, the CASSCF geometry for the $^3B_2$ state has a much shorter C2−N4 bond length (1.330 Å) than that of the corresponding ROHF geometry (1.418 Å).[29] On the other hand, the C2−N4 bond length of the $^1A_1$ state slightly changes through the CASSCF reoptimization. On the whole, the skeleton of the central triazine moiety preserves the typical structure of triazine ring[30] for all the states.

At the ROHF/GVB level, the $^3B_2$ and $^1A_1$ states are nearly degenerate to lie about 20 kcal/mol below the $^1B_2$ state. However, at the CASSCF level of calculation, the $^3B_2$ state is predicted to be the ground state of $\mathbf{2}^{2+}$; the $^1B_2$ and $^1A_1$ states lie 13.1 and 34.9 kcal/mol, respectively, above the $^3B_2$ state. At the CASSCF//CASSCF level, the $^1A_1$ state finally becomes the lowest singlet state lying below the $^1B_2$ state by 5.7 kcal/mol. This is because there is a pronounced change in the fractional occupation numbers of the active orbitals in going from the CASSCF//GVB level (1.98, 2.00, 1.93, 1.08, 0.92, 0.06, 0.02, 0.02) to the CASSCF//CASSCF level (1.95, 1.90, 1.89, 1.11, 0.91, 0.10, 0.10, 0.04). The GVB calculations are, therefore, not appropriate for describing the $^1A_1$ state of $\mathbf{2}^{2+}$. As a result, the $^3B_2$ state remains the ground state of $\mathbf{2}^{2+}$ lying below the lowest singlet by 12.8 kcal/mol.

At this juncture, the existence of the other triplet states of $\mathbf{2}^{2+}$ is worth passing mention. This is because the electron configuration for diamino-1,3,5-triazine in C_{2v} symmetry is $|...10b_2^2 14a_1^2 3b_1^2 2a_2^2\rangle$, where $10b_2$ and $14a_1$ are σ lone-pair orbitals on the three N atoms of the 1,3,5-triazine ring. This suggests the possibility of σ- and π-mixed diradicals. We have performed the geometry optimization of the $^3A_2$ ($=|...14a_1^1 2a_2^1(\alpha\alpha)\rangle$) and $^3B_1$ ($=|...10b_2^1 2a_2^1(\alpha\alpha)\rangle$) states at the ROHF/6-31G* level. As shown in Figure 2, the σ-framework of the central 1,3,5-triazine ring is considerably deformed from the usual one, so that each state has a σ- and π-mixed diradical character. However, the $^3A_2$ and $^3B_1$ states are rather

(28) Net charges for the $^3B_2$ states of $\mathbf{1}^{2+}$ and $\mathbf{2}^{2+}$. $\mathbf{1}^{2+}$: C1 (+0.16), C2 (+0.15), C3 (−0.42), C4 (+0.12), N1 (+0.81). $\mathbf{2}^{2+}$: C1 (−0.35), N1 (+0.44), C2 (−0.78), N2 (+0.52), N4 (+0.49). The other states of $\mathbf{1}^{2+}$ and $\mathbf{2}^{2+}$ have similar charge distribution except for the $^1A_1$ state of $\mathbf{1}^{2+}$ (see text).

(29) In order to justify these noticeable changes, it may be necessary to perform further geometry reoptimizations including σ−π correlation.

(30) Pyckhout, W.; Callaerts, I.; Van Anselroy, C.; Geise, H. J.; Amenningen, A.; Seip, R. *J. Mol. Struct.* **1986**, *147*, 321−329. Wiberg, K. B.; Nakaji, D.; Breneman, C. M. *J. Am. Chem. Soc.* **1989**, *111*, 4178−4190. Creuzert, S.; Langlet, J. *Chem. Phys. Lett.* **1993**, *208*, 511−516.

Table 4. Calculated Atomic Spin Densities and Proton and Nitrogen Isotropic Hyperfine Coupling Constants a^N (G) for the $^3B_2$ States of 1^{2+} and 2^{2+}

	B3LYP/6-31G*// CASSCF/6-31G*	B3LYP/6-31G*// B3LYP/6-31G*
$\mathbf{1}^{2+}$		
C1	−0.16	−0.16
C2(C6)	+0.45	+0.43
C3(C5)	−0.08	−0.09
C4	+0.72	+0.69
N1(N2)	+0.42	+0.45
a^{H1}	+2.58	+2.55
a^{H2}	−11.57	−11.25
a^{H3}	−11.86	−12.64
a^{H4}	−11.63	−12.41
a^{H5}	−17.52	−16.99
a^{N1}	+7.64	+8.46
$\mathbf{2}^{2+}$		
C1	−0.20	−0.20
N1(N3)	+0.41	+0.41
C2(C3)	−0.18	−0.19
N2	+0.52	+0.52
N4(N5)	+0.65	+0.66
a^{H1}	+3.70	+3.86
a^{H2}	−17.03	−17.32
a^{H3}	−16.90	−17.18
a^{N1}	+6.21	+6.22
a^{N2}	+7.98	+8.05
a^{N4}	+11.29	+11.74

high, lying 21.4 and 50.6 kcal/mol, respectively, above the $^3B_2$ state at the ROHF/6-31G* level.

The spin densities on $\mathbf{1}^{2+}$ and $\mathbf{2}^{2+}$ in the $^3B_2$ states are important values to study intra- and intermolecular magnetic interactions. It is often said that density functional theory (DFT) calculations[31] give good results for both signs and magnitudes of spin densities of open-shell molecules.[32] We performed calculations using a hybrid HF/DF method (B3LYP) that combines Becke's three-parameter nonlocal exchange functional[33] with the nonlocal correlation functional of Parr *et al.*[34] at each CASSCF geometry of the triplet states of $\mathbf{1}^{2+}$and $\mathbf{2}^{2+}$.[35] Although the reoptimizations were carried out using the B3LYP method, there were not any notable differences between the CASSCF and the B3LYP optimized geometries. The calculated spin densities on the triplet states of $\mathbf{1}^{2+}$ and $\mathbf{2}^{2+}$ are listed in Table 4. Apparently, our calculations show a spin-polarized pattern. As expected by the qualitative MO considerations indicated in Figure 1, the spin density on $\mathbf{1}^{2+}$ is delocalized mainly on the benzene ring. In particular, the large spin-density at the *ortho* and *para* carbons to the amino groups of $\mathbf{1}^{2+}$ is disadvantageous to the realization of stable high-spin molecules.[36] On the other hand, in the lowest $^3B_2$ state of $\mathbf{2}^{2+}$, the spin densities are localized at the peripheral N atoms, in contrast with the $^3B_2$ state of $\mathbf{1}^{2+}$. This suggests the possibility of high chemical stability of a 1,3,5-triazine ring. Furthermore, we find that the spin densities are polarized more on the triazine ring of $\mathbf{2}^{2+}$ than on the benzene ring of $\mathbf{1}^{2+}$, which may suggest a stronger ferromagnetic coupling in $\mathbf{2}^{2+}$.

We next look at hyperfine coupling constants (hfcc). Their values are related directly to electron spin density at the nucleus according to the equation shown below

$$a_{\mathrm{iso}}^{\mathrm{N}} = \frac{8\pi}{3} g\beta g_{\mathrm{N}}\beta_{\mathrm{N}}\rho(\mathbf{r}_{\mathrm{N}})$$

where g is the electronic g value, β is the Bohr magneton, g_N and β_N correspond to those for the nucleus N, and $\rho(\mathbf{r}_N)$ is the Fermi contact integral. We can evaluate the latter term by using the relation

$$\rho(\mathbf{r}_{\mathrm{N}}) = \sum_{\mu\nu} \mathbf{P}_{\mathrm{mn}}^{\alpha-\beta}\phi_\mu(\mathbf{r}_{\mathrm{N}})\phi_\nu(\mathbf{r}_{\mathrm{N}})$$

where $\mathbf{P}^{\alpha-\beta}$ is a one-electron spin density matrix, the summation runs over all atomic basis functions μ and ν, and the product of orbitals $\phi_\mu(\mathbf{r}_N)$ and $\phi_\nu(\mathbf{r}_N)$ is computed at the nuclear position $\mathbf{r}_N$.

The spin density at the hydrogen nucleus depends most strongly upon the spin polarization of electrons in the C−H or N−H σ bonds by unpaired carbon or nitrogen π electron density, and therefore, it is of significance in the charged and highly spin-polarized systems. Specifically, gradient-corrected DF methods[31] and hybrid HF/DF methods[31] were reported to yield more accurate hfcc's for organic radicals.[37] Moreover, Qin and Wheeler recently showed that these DF methods yield hfcc's for the phenol radical cation in adequate agreement with experiment.[38] Table 4 also shows the signs and magnitudes of proton and nitrogen hfcc's calculated by the B3LYP method for $\mathbf{1}^{2+}$ and $\mathbf{2}^{2+}$. In diarylaminiums, the coupling constants are known to vary gradually according to the difference in the substituted groups, with a^N (7.41−9.17 G) and $a^{H_{NH}}$ (9.15−11.14 G).[39] The comparison between these experimental values and the DFT-derived hfcc's, in particular, a^{N1}, a^{H3}, and a^{H4}, implies that the B3LYP method gives reasonable spin properties for $\mathbf{1}^{2+}$.

Finally, let us look at the singlet−triplet splitting (ΔE_{S-T}) of *m*-QDM, $\mathbf{1}^{2+}$, and $\mathbf{2}^{2+}$. At the CASSCF//ROHF (or GVB) level (Table 3), those of $\mathbf{1}^{2+}$ and $\mathbf{2}^{2+}$ are calculated to be 10.2 and 13.1 kcal/mol, respectively. In contrast with the value 10.8 kcal/mol for *m*-QDM,[40] this shows that an *m*-1,3,5-triazinediyl coupler can effectively enhance the ferromagnetic interaction between aminium radical centers, while the nitrogen-substitution (**1**) of the peripheral carbons of *m*-QDM does not change the value of ΔE_{S-T}. This tendency is still maintained at the CASSCF//CASSCF level. The CASSCF treatment contains nondynamic electron correlation such as the energetic near-degeneracy of Slater determinants, but not dynamic correlation. Thus, we computed the energies of $\mathbf{1}^{2+}$ and $\mathbf{2}^{2+}$ by using the CASPT2 method, a multiref-

(31) For a recent review of DFT methods see: Kohn, W.; Becke, A. D.; Parr, R. G. *J. Phys. Chem.* **1996**, *100*, 12974−12980.

(32) See, for instance: Zheludev, A.; Barone, V.; Bonnet, M.; Delly, B.; Grand, A.; Ressouche, E.; Day, P.; Subra, R. Schweizer, J. *J. Am. Chem. Soc.* **1994**, *116*, 2019−2027.

(33) Becke, A. D. *J. Chem. Phys.* **1992**, *96*, 2155−2160; **1992**, *97*, 9173−9177; **1993**, *98*, 5648−5652.

(34) Lee, C.; Yang, W.; Parr, R. G. *Phys. Rev. B* **1988**, *37*, 785−789.

(35) In all the DFT calculations, the $\langle S^2\rangle$ values were very close to the exact value 2.0 required for the triplet state.

(36) The new bond formation at the *ortho* and *para* positions is frequently pointed out to be the main culprit in the kinetic instability of arylaminium radicals. See, for example: Reynolds, R.; Line, L. L.; Nelson, R. F. *J. Am. Chem. Soc.* **1974**, *96*, 1087−1092.

(37) Eriksson, L. A.; Malkin, V. G.; Malkina, O. L.; Shalahub, D. R. *Int. J. Quantum Chem.* **1994**, *52*, 879−901. Eriksson, L. A.; Malkina O. L.; Malkin, V. G.; Shalahub, D. R. *J. Chem. Phys.* **1994**, *100*, 5066−5075. Adamo, C; Barone, V; Fortunelli, A. *J. Chem. Phys.* **1994**, *98*, 8648−8652. Ishii, N; Shimizu, T. *Phys. Rev. A* **1993**, *48*, 1691−1694. Ishii, N; Shimizu, T. *Chem. Phys. Lett.* **1994**, *225*, 462−466. Cohen, M. J.; Chong, D. P. *Chem. Phys. Lett.* **1995**, *234*, 405−412. Oliphant, N.; Bartlett, R. J. *J. Chem. Phys.* **1994**, *100*, 6558−6561. Qin, Y.; Wheeler, R. A. *J. Chem. Phys.* **1995**, *102*, 1689−1698. Qin, Y.; Wheeler, R. A. *J. Am. Chem. Soc.* **1995**, *117*, 6083−6092.

(38) Qin, Y.; Wheeler, R. A. *J. Phys. Chem.* **1996**, *100*, 10554−10563.

(39) Neugebauer, F. A.; Bamberger, S. *Angew. Chem., Int. Ed. Engl.* **1971**, *10*, 71.

(40) Fang, S.; Lee, M.-S.; Hrovat, D. A.; Borden, W. T. *J. Am. Chem. Soc.* **1995**, *117*, 6727−6731.

erence version of the second-order many-body perturbation theory developed recently by Roos *et al.*[41] At this higher *ab initio* MO level, the ΔE_{S-T} for $\mathbf{1}^{2+}$ is dramatically reduced to 0.7 kcal/mol, due to the large dynamic correlation for the $^1A_1$ state, while that for $\mathbf{2}^{2+}$ is almost unchanged (ΔE_{S-T} = 12.5 kcal/mol).[29] As described earlier, the $^1A_1$ state exhibits a cyanine-like distortion, and therefore, has a highly ionic character compared with the $^3B_2$ and $^1B_2$ states. On the other hand, in $\mathbf{2}^{2+}$, charge polarization is reduced by dispersion over the triazine ring due to aza-substitution onto *m*-phenylene. Hence, the highly ionic character of the $^1A_1$ state of $\mathbf{1}^{2+}$ explains why this state is significantly stabilized by dynamic correlation compared with the other states of $\mathbf{1}^{2+}$ and $\mathbf{2}^{2+}$. In conclusion, *m*-1,3,5-triazinediyl is an effective ferromagnetic coupler for aza-substituted systems. Our prediction of triplet ground states for $\mathbf{1}^{2+}$ and $\mathbf{2}^{2+}$ awaits experimental verification.[42]

Acknowledgment. This work was supported by a Grant-in-Aid for Scientific Research from the Ministry of Education, Science and Culture of Japan and the JSPS Program of Research for the Future. A.I. is grateful to the Research Fellowships of the JSPS for Young Scientists for financial support. Numerical calculations were carried out at the Supercomputer Laboratory of the Institute for Chemical Research of Kyoto University.

JO9610319

(41) Anderson, K; Malmqvist, P.-Å.; Roos, B. O. *J. Chem. Phys.* **1992**, *96*, 1218−1226.

(42) Bisaminyl derivatives of *m*-QDM are, however, known: Schaffer, M.; Platz, M. S. *Tetrahedron Lett.* **1989**, *30*, 1225−1228.